First results on a new PIAA coronagraph testbed at NASA Ames

Ruslan Belikov[*a], Eugene Pluzhnik[a], Michael S. Connelley[a], Fred C. Witteborn[a], Dana H. Lynch[a],
Kerri L. Cahoy[a], Olivier Guyon[b], Thomas P. Greene[a], Mark E. McKelvey[a]
[a]NASA Ames Research Center, Moffett Field, CA;
[b]National Astronomical Observatory of Japan / Subaru Telescope, Hilo, HI.

ABSTRACT

Direct imaging of extrasolar planets, and Earth-like planets in particular, is an exciting but difficult problem requiring a telescope imaging system with 10^{10} contrast at separations of 100mas and less. Furthermore, the current NASA science budget may only allow for a small 1-2m space telescope for this task, which puts strong demands on the performance of the imaging instrument. Fortunately, an efficient coronagraph called the Phase Induced Amplitude Apodization (PIAA) coronagraph has been maturing and may enable Earth-like planet imaging for such small telescopes. In this paper, we report on the latest results from a new testbed at NASA Ames focused on testing the PIAA coronagraph. This laboratory facility was built in 2008 and is designed to be flexible, operated in a highly stabilized air environment, and to complement existing efforts at NASA JPL. For our wavefront control we are focusing on using small Micro-Electro-Mechanical-System deformable mirrors (MEMS DMs), which promises to reduce the size of the beam and overall instrument, a consideration that becomes very important for small telescopes. At time of this writing, we are operating a refractive PIAA system and have achieved contrasts of about 1.2×10^{-7} in a dark zone from 2.0 to 4.8 λ/D (with 6.6×10^{-8} in selected regions). In this paper, we present these results, describe our methods, present an analysis of current limiting factors, and solutions to overcome them.

Keywords: extrasolar planets, high contrast, coronagraph, PIAA, wavefront correction

1. INTRODUCTION

Direct imaging and spectral characterization of an Earth-like extrasolar planet (exo-Earth) is one of the most exciting goals in astrophysics, one that appeals as much to the layman as to the scientist, one with lasting ramifications, and one that may be possible to achieve in the coming decade with a space telescope as small as 1.4m.

A technology that can enable this is the Phase-Induced Amplitude Apodization (PIAA) coronagraph [1-4], which can provide contrast levels of 10^{10} at an inner working angle of 2 λ/D with theoretically almost no loss of throughput. A schematic of the PIAA coronagraph is shown in Figure 1. The heart of the coronagraph is a pair of aspheric optics (mirrors or lenses) that reshape the original uniformly illuminated telescope pupil into an apodized pupil shape. The shape of this apodized pupil is specially designed such that its Fourier Transform (or PSF in the focal plane) is a concentrated dot with no Airy diffraction rings down to the desired contrast level. The pair of PIAA optics is usually augmented by a (high-throughput) classical apodizer mask to facilitate manufacturing as well as to prevent undesirable chromatic diffraction effects [5]. A hard-edge focal plane occulter is also usually used to prevent undesirable artifacts on the CCD from the bright star.

PIAA performance is close to the theoretical limit of any possible coronagraph [6], which potentially enables imaging of exo-Earths around nearby stars with relatively small visible-light space telescopes such as the Pupil-mapping Coronagraphic Observer (PECO, see Figure 1, Figure 2, as well as companion papers [7,8]). It also scales very well to even smaller and cheaper missions such as a telescope on a balloon (though these are no longer able to image Earths), or larger ones such as a Terrestrial Planet Finder flagship mission. PIAA is also starting to be used on ground telescopes, namely the Subaru telescope.

PIAA has a successful track record of hardware development and testing, and is steadily progressing toward maturity. A number of lens and mirror sets have been manufactured, with the latest set believed to be able to provide 1e-9 contrast across a 10%-wide spectral band according to simulations that take into account known manufacturing errors. Initial

---

*[*] Ruslan.belikov@nasa.gov, 650-604-0833

PIAA prototyping and testing had been going on at the Subaru coronagraph testbed for the past three years, culminating with the demonstration of 2.3×10^{-7} contrast between 1.65 and 4 λ/D in monochromatic light [9].
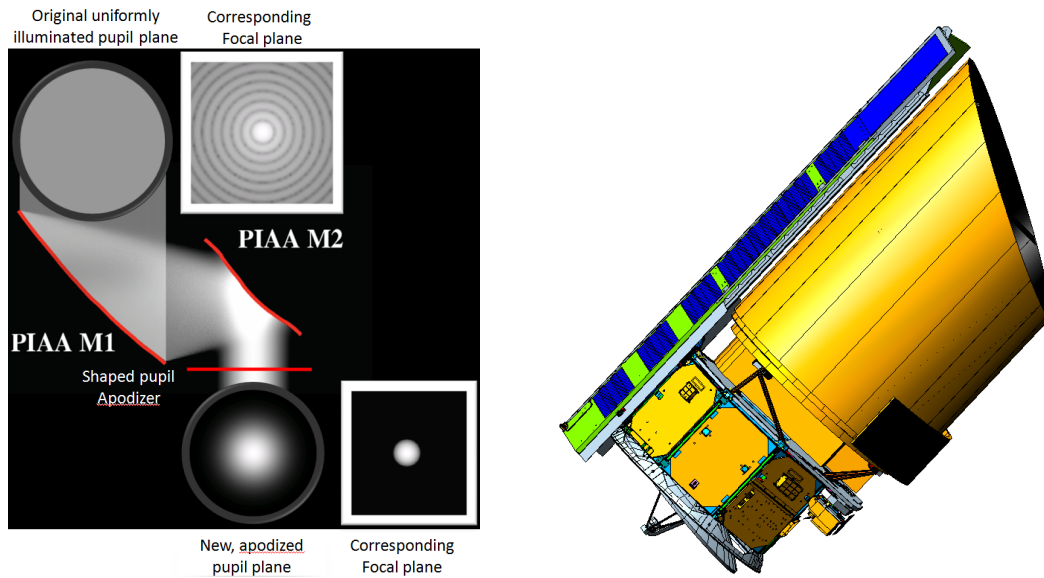

Figure 1. Left: principle of the PIAA coronagraph. Right: proposed PECO telescope.

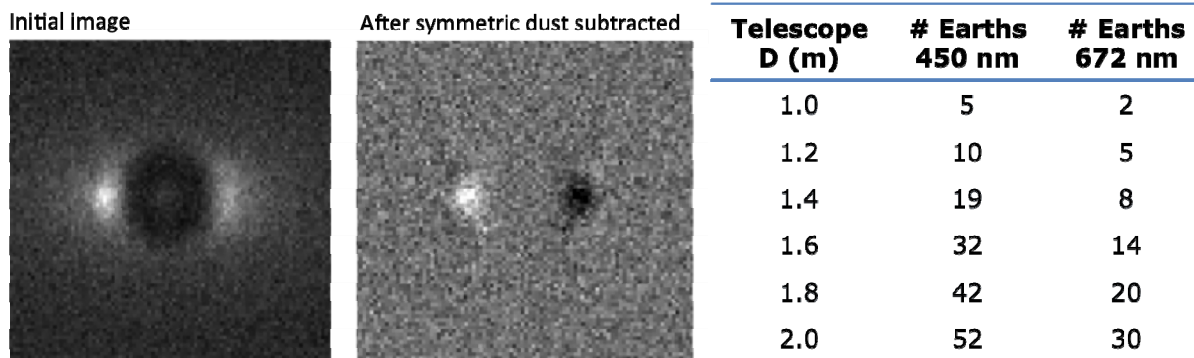| Telescope D (m)	# Earths 450 nm	# Earths 672 nm
1.0	5	2
1.2	10	5
1.4	19	8
1.6	32	14
1.8	42	20
2.0	52	30

Figure 2. *Left and center*: Simulated PECO images of an Earth-like planet around Tau Ceti in a 500-600nm band with an exozodi comparable to the solar system. Photon noise and 16 electrons total detector noise for an electron multiplying CCD have been added. *Right*: Simulated performance of PECO at different wavelengths and telescope diameters.

Continued development and testing of PIAA is being transferred to a more stable testbed at NASA Ames and vacuum High Contrast Imaging Testbed (HCIT) at JPL. The remaining path to full maturity of PIAA has been laid out in white papers submitted to the astro2010 decadal survey [10,11], which describe a plan based on a synergy of the testbeds at Ames and JPL. The Ames testbed is designed to be flexible and cheap, operated in air, with quick turn-around of experiments, and will be used for prototyping lower-TRL technologies related to PIAA such as new wavefront control architectures, MEMS DMs, and feasibility of using dichroics to split high contrast spectral channels. Once sufficiently mature, these will subsequently undergo final vacuum testing at JPL's High Contrast Imaging Testbed (HCIT).

In this paper, we describe the results of the first year of the Ames testbed operations. In particular, the contrast level achieved to date on the Ames testbed is 1.2×10^{-7}, spatially averaged between 2.0 and 4.8 λ/D. (See companion paper [12] for a description of complementary PIAA testing at JPL's HCIT that has been going on in parallel.) In particular,

Chapter 2 focuses on the description of our testbed and hardware, and Chapter 3 describes our experimental results and limiting factors.

2. ARC TESTBED DESCRIPTION

2.1 General description

The Ames coronagraph testbed is a new facility designed for development and testing of the PIAA coronagraph. It began operations in March '08 (although wavefront control did not start till August). It is essentially a successor to the original PIAA testbed at Subaru [9], and is designed with several improvements from lessons learned at Subaru, in particular with regard to stability and reconfigurability. It is operated in an air environment (as opposed to vacuum) to make accessing and reconfiguring the layout easier and cheaper, complementing the vacuum HCIT facility.
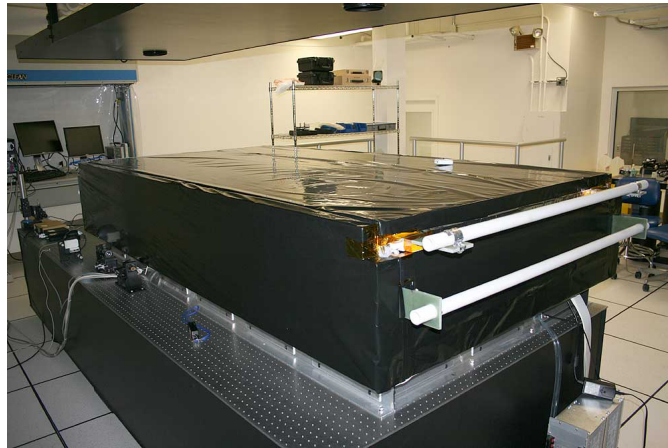

Figure 3. Photograph of the Ames optical bench and enclosure, which was designed to minimize thermal flexure and air motion.

One of the difficulties in working in an air environment is thermal instabilities and air motion. Experience in many different coronagraph labs in air shows that without special precautions, thermal and air instabilities create speckle instabilities at about 10^{-6} or 10^{-7} contrast levels, although this depends on the inner working angle (smaller is worse), beam sizes (smaller is better), and time interval (shorter is better). Therefore, stability was an important consideration in the design of the Ames testbed environment. In particular, our optical bench is 2' thick and has a lot of thermal inertia (see Figure 3). Our enclosure has layers of thermal isolation and a minimum of gaps. We are currently achieving a temperature stability of ~10mK rms over 20 minutes (this length of time is the expected duration of our wavefront control loop at 10^{-9} contrast), and speckle intensity variations are about 10^{-8} in 20 minutes. We are also in the process of building an active thermal control system to improve stability even more, based on an earlier version at the Subaru testbed. The control of temperature will be achieved by introducing a water circuit in our enclosure and actively controlling the temperature of the water flowing through that circuit.

2.2 Optical layout

The current optical layout of our testbed is shown in Figure 4. The light source is a long-coherence-length 650nm laser coupled into a single mode fiber. The fiber output serves as a reasonable approximation to a star (except for being monochromatic). This light is then collimated by a 50mm focal length lens into an almost uniformly illuminated beam, which passes through our refractive PIAA system (see next section), then gets reflected by a DM, focused onto a focal plane occulter, and reimaged onto the CCD.

Note that our layout is a simplified version of what a final PIAA-based system will look like. For example, the PECO PIAA system uses reflective components to reduce chromatic effects and prevent ghosts, and uses 2 DMs with one of them conjugated to one of the PIAA optics, partially to help with correcting chromatic error. However, our approach is

to first demonstrate a simplified system in monochromatic light, and then move to a broadband system. Our initial goals are to develop and measure the stability of our environment, as well as demonstrate the needed accuracy and stability of the DM, which can be accomplished just as well in monochromatic light as in broadband.
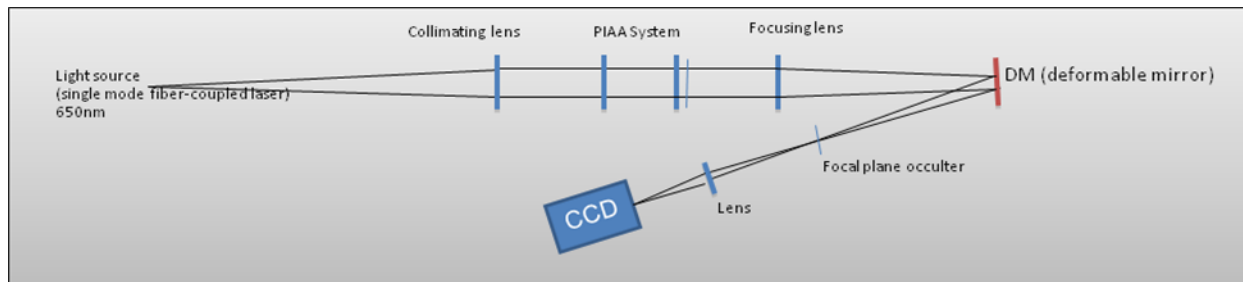

Figure 4. Default optical layout of the experiments on the Ames testbed. (Some experiments and measurements have slight differences from this as noted in the corresponding text.)

Furthermore, working in monochromatic light enables us to better isolate, study, and remove the effects that occur at any given wavelength from those that are purely chromatic, in a "divide-and-conquer" strategy. Since we are working in monochromatic light, chromaticity is not an issue and ghosts can be removed by a DM just as if they were a speckle caused by an aberration (provided the coherence length of the laser is long enough). This enables a cheap and simple lens-based system in Figure 4 that is easier to align and operate but does not compromise on delivering our desired measurements such as system stability and DM performance. That being said, broadband tests with PIAA mirrors are of course critically important and have been started at HCIT, which is described in a companion paper ([12]).

2.3 PIAA system

The design of a PIAA system is relatively straightforward. A desired apodization is chosen to be either a prolate spheroidal function, (as in the design described in [3]), or a numerically optimized one (as in the design described in [4]), and then a set of differential equations is numerically solved to obtain the mirror shapes [1,2], at least for the case of an on-axis system such as lenses. (For the case of mirrors, which are off-axis, an off-axis term as well as certain corrections must be added.) However, desired apodization functions are usually 0 at the aperture edge, which leads to an infinite radius of curvature on the optics at the edge (which is practically unmanufacturable), as well as certain chromatic diffraction problems [5]. Therefore, typically the apodization required of the lenses is relaxed by limiting the lowest apodization value to some small but non-zero value, and then augmenting the PIAA lens or mirror system by following it with a classical apodizer (shaped pupil) that recovers the desired apodization with a very slight (typically 10%) loss of throughput. Extensive literature has been published on shaped pupil designs by optimization methods (e.g. [13]). Thus, all practical PIAA systems are actually hybrids of a "pure PIAA" and a shaped pupil coronagraph, and there is a spectrum of possible designs ranging from pure shaped pupils on one end and pure PIAA on the other. Different points on this spectrum correspond to what share of the apodization is accomplished by the PIAA system versus the shaped pupil, and represent a trade-off between manufacturability of the PIAA and performance of the system in terms of throughput and inner working angle.

Lenses
The manufactured designs to date put more weight on the pure PIAA part of the system to provide performance that is close to 100% throughput and a very good inner working angle. Consequently, the PIAA lenses and mirrors are quite aspheric and challenging to manufacture, but manufacturing maturity has been steadily progressing, culminating in a set of mirrors manufactured by Tinsley, which is believed to achieve 10^{-9} contrast in a 10% band according to simulations that take into account known errors. However, as mentioned in section 2.1, our first series of tests employ a lens-based system in monochromatic light.

PIAA lenses are about an order of magnitude simpler and cheaper to manufacture than mirrors because they are on-axis and thus rotationally symmetrical, and because they are usually designed for monochromatic lab tests or not very aggressive contrasts for ground-based applications, leading to relaxed optical quality requirements. Many different lens sets have been manufactured at Axsys by diamond turning calcium fluoride. Figure 5 shows the set that has been used at Ames for the experiments described in this paper. They have an active diameter of 16mm (on a 1" substrate). For certain

mostly historical reasons this PIAA system was designed for 10^8 contrast at 2 λ/D, although we are intending to upgrade to our 10^{10} contrast set, or the Tinsley mirrors, once we reach the contrast limit of the current lens set.
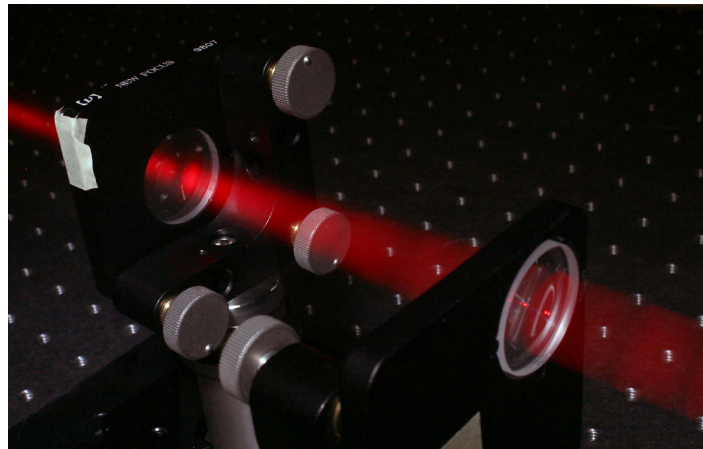

Figure 5. PIAA lens system showing the remapping of a uniformly illuminated 16mm beam into a high contrast apodized beam

Even though the baseline PECO PIAA design calls for mirrors in order to avoid problems with chromaticity and ghosts in lenses, an intriguing possibility is to develop a lens with achromaticity and AR-coatings sufficient for 10^{10} contrast (after correction). This potentially enables savings in size and cost of the final system, as well as ease of design, setup, and alignment.

Apodizer

The apodizer for our system is a concentric-ring apodizer designed using a method developed by Vanderbei [13] and is shown in Figure 6. The method expresses apodizer design as constrained linear optimization problem and then solves it using the LOQO solver in AMPL. Specifically, the apodizer is expressed as an array representing its sampled radial profile, and those samples are optimized for maximum apodizer throughput under the constraints that the PSF be lower than the desired contrast between the desired inner and outer working angles. For the apodizer we are using in this paper, the contrast was chosen to be 10^{-8}, and the inner and outer working angles of 2 and 20 λ/D (on the sky), respectively. We also used the additional constraints that the apodizer be fully transmissive in the 30% of its center and totally opaque in the outer 10% of its radius. The latter helps with avoiding edges of the mirrors which are prone to errors due to manufacturing or misalignment, and the former helps to attenuate light in the region where the gradient is not too strong (making the system less sensitive to apodizer misalignment), and the attenuation happens where the light is already dim.
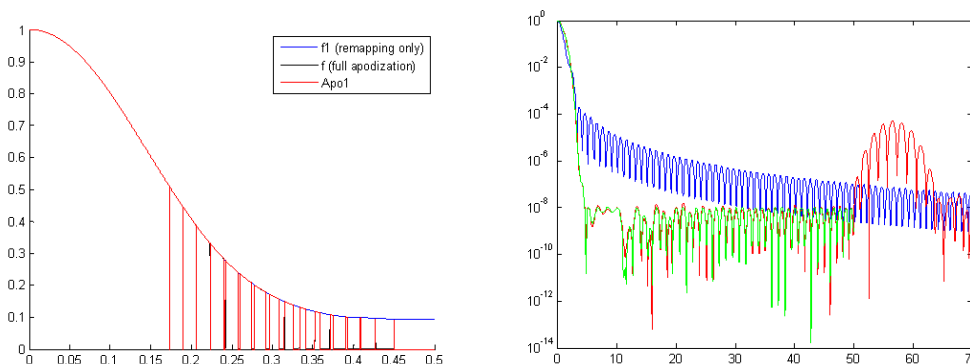

Figure 6. Left: Pupil plane plots of field amplitude after the pure PIAA remapping (blue) and after the apodizer (red and black, corresponding to two different computational methods). Right: Corresponding intensity PSFs (Green and red are two different computational methods).

Binary apodizers are usually preferable to continuous ones because they are easier to make and are less chromatic. However it turns out that the optimization scheme described above already converges to binary shapes (i.e. 0 or 1 valued) without the need to specifically require that. Our apodizer has 17 rings with the smallest feature being 10 microns wide and is relatively straightforward to manufacture. It was manufactured at JPL's Microdevice lab by depositing aluminum on a wedged piece of glass.

Note that formally, the apodizer design assumes that the apodizer is in the plane of the second PIAA lens (PIAA L2), so that they should lie in conjugate planes. However, simulations show that they can be out of conjugation by at least 5cm (measured along a collimated beam) without affecting the PSF at the 10^{10} contrast level. So, in our layout we did not conjugate the apodizer to PIAA L2, but rather placed it close (~5cm) downstream from it.

Focal plane occulter

The focal plane occulter blocks the concentrated starlight from reaching the CCD while letting the dark zone pass through. It is not necessary in theory, because light from the star will be completely spatially separated from any planets in the dark zone as long as the wavefront control system is working well. In fact, we originally had no focal plane occulter and had our CCD at first focus, in the location of the focal plane occulter. This ultimately proved unworkable because we observed many CCD artifacts at the 10^{-5} - 10^{-6} level at our inner working angle. These seem to be caused by scatter of either photons or electrons in the CCD electronics, effectively creating cross-talk between pixels. We also observed increased artifacts on those CCDs that have microlenses, and non-negligible scatter from the CCD shutter. Furthermore, blooming can be a problem, even with CCDs that have anti-blooming if the image has dynamic range of 10^{10}.

Nevertheless, being able to use a CCD at first focus actually has a lot of benefits: it reduces the number of optics in the system and any aberrations associated with those optics, it lets you see the entire PSF and thus makes it easier to correct low-order aberrations that occur at or inside the inner working angle, and it eliminates certain problems related to diffraction off the edge of the focal plane stop that we will describe later. But, this requires a CCD that is free of artifacts when presented with an image that has a dynamic range of 10^{10}. To our best knowledge, no such CCD exists and thus we resort to blocking the light with a focal plane occulter. (Although a focal plane occulter can actually be useful when used as part of the low-order wavefront sensor [14].)

The focal plane occulter we used for the experiments described in this paper is a chrome disk with a radius of 96 microns (corresponding to 2 λ/D inner working angle) on a substrate of quartz, made by HTA Photomask. The optical density of the chrome layer is 5, so that everything inside 2 λ/D is not completely blocked, but rather attenuated by a factor of 10^5. This enables us to see our "star" in every image without it overwhelming the dark zone, and is useful as one way to calibrate its variations in brightness and position.

2.4 Motivation for and description of the MEMS Deformable mirror

One of the initial goals of our testbed is to demonstrate the viability of MEMS deformable mirrors for space-based exoplanet imaging. One strong motivation for this is that MEMS DMs are quite compact and can reduce the size of the instrument. For example, in the PECO mission baseline, there are 8 deformable mirrors in the final instrument (4 spectral channels with 2 DMs per channel). If these DMs are large, they can drive the beam size and instrument size. If the telescope is as small as PECO (1.4m), the instrument can swell to be larger than the telescope itself and drive the cost of the mission. Even in large missions small DMs are probably desirable because missions are often mass constrained. Another motivation is that MEMS DMs are relatively cheap because they make use of very mature IC manufacturing technology and can be made in bulk; and are also widely available from several different vendors at present.

The DM we are using on our testbed was manufactured by Boston Micromachines. It consists of a grid of 32 x 32 actuators in a 10cm square aperture. It also has a protective window on it (for broadband tests a DM without such a window will probably be used). The actuation is through electrostatic capacitive attraction. It has no bad actuators.

2.5 Alignment procedures

Any PIAA system is quite sensitive to misalignment and all its components must be aligned carefully and precisely. After roughly aligning all the optics to a laser beam, the fine alignment procedure we use is based on iterative adjustments of all the components in the direction that maximizes the sharpness of the PSF on the CCD (without the focal plane occulter). This simple procedure has proved to work pretty well, because the different misalignment modes are not fully degenerate. It is also possible to use a more complex but faster model-based procedure that computes the

misalignments based on decomposing PSF distortions into misalignment modes, thus measuring them simultaneously and removing them directly. (This procedure may be necessary for the alignment of mirrors where there is more degeneracy.)

3. EXPERIMENTAL RESULTS

3.1 Initial testing, calibration, and comparison to models

Several calibrations are necessary both for accurate measurements of contrast and inner working angle, as well as to measure the parameters necessary for wavefront control.

The most basic measurement is a test of how closely the actual apodization and the focal plane PSF matches the model. This is important for one of the wavefront control algorithms (EFC, see below), as well as a check of both alignment and models. The plane of the "actual apodization" is approximately the plane of the apodizer. (Technically, since our apodizer is not in the plane of the second PIAA lens (PIAA L2), we never quite get our desired apodization, but the difference is negligible according to models). However, for purposes of wavefront control, the DM plane is much more relevant than the plane of the apodizer. To model the field in the DM plane, we started with the theoretical error-free field at PIAA L2 and Fresnel-propagated it through the apodizer and the focusing lens to the DM plane. The result is shown in Figure 7. Note that the "apodization" on the DM is now a somewhat rippled version of the desired apodization, representing the diffraction between the apodizer and DM planes. However, this of course does not degrade the PSF and in fact mathematically the intensity of the PSF obtained by Fourier-transforming the DM plane field is exactly the same as the desired one obtained by Fourier-transforming the original desired apodization. (This is not a contradiction because the fields of the two PSF fields thus obtained are not the same, but differ by a quadratic phase factor, which can usually be ignored.)
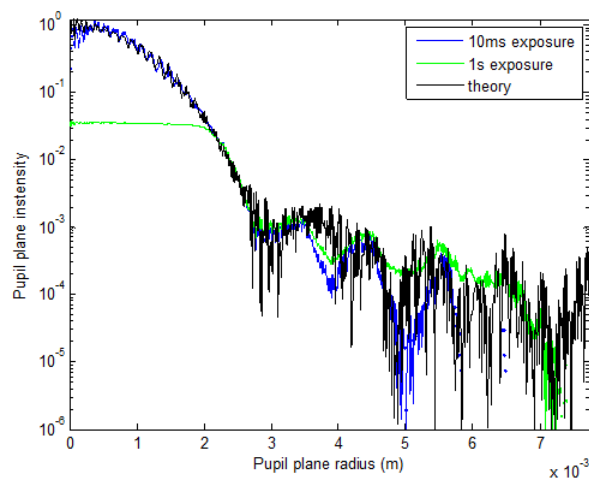

Figure 7. Comparison of models to measurements in the plane of the DM, validating the hardware and models.

We then took an image of the intensity on the DM (by introducing a lens in our layout that reimages the DM onto the CCD), and took a radial average to obtain a function of radius only. The results are plotted in Figure 7 against the model. The fit in the range 0.3mm < r < 3.5mm is good. The discrepancy in the r < 0.3mm range may be due to a combination of print-through aberrations on the DM and fewer number of points to average out those aberrations in the radial average; and the discrepancy beyond 3.5mm is due to photon noise and aberrations on the edge of the beam. However, overall the fit validates that the shapes of the PIAA optics, apodizer, their alignment, and our models are all reasonably correct.

A comparison of measurements to models in the focal plane is shown in Figure 8 (CCD images) and Figure 9 (horizontal slices). These tests were designed to validate both the on-axis PSF as well as the off-axis magnification inherent in PIAA, and were performed without the focal plane occulter (and with the CCD in the plane of the FPO). Also, to reduce errors, the apodizer was removed and the DM was replaced by a flat mirror. (Tests with the apodizer and DM were also performed on-axis and did not show appreciable differences).
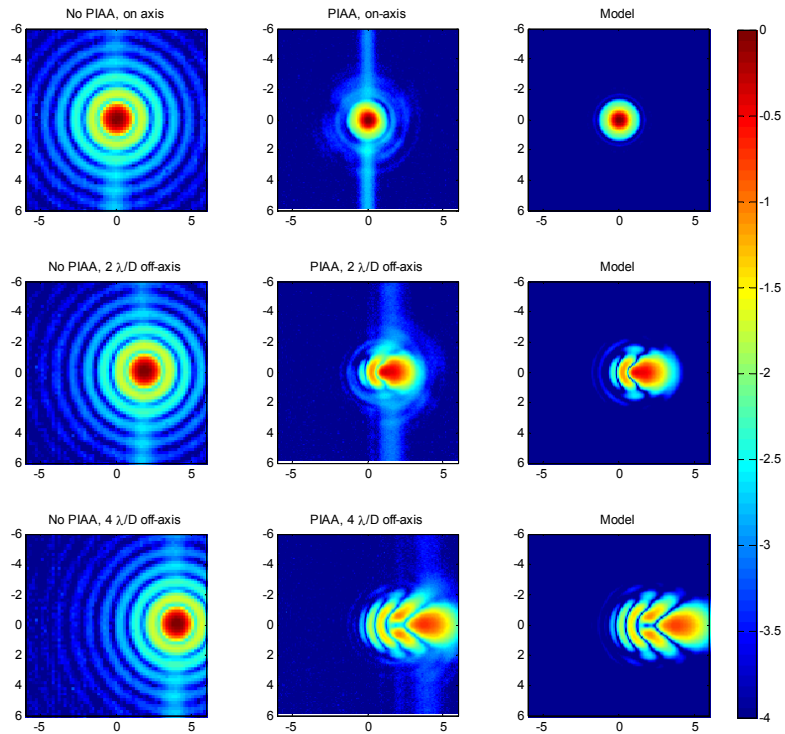
Figure 8. Comparisons of on-axis and off-axis focal plane CCD images to models. The x,y scale in all images is in units of λ/D on the sky, and the brightness scale is a logarithm base 10. The vertical lines in images are CCD artifacts. (Also note that due to PIAA magnification of 2.72, the actual size of the leftmost column on the CCD is 2.72 times smaller than the other columns)
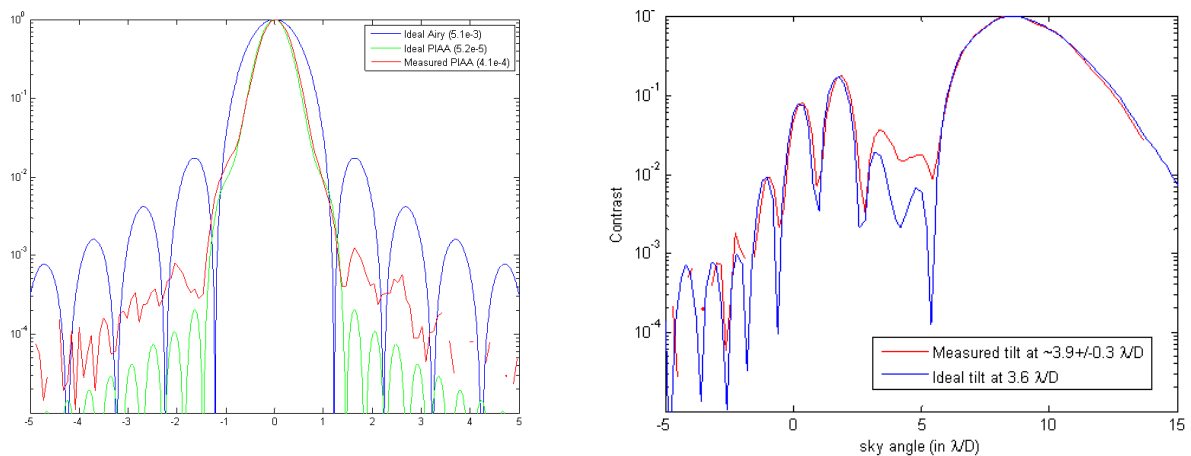

Figure 9. Comparison of measurements of PIAA PSFs against models. Left: on-axis. Right: off-axis. (Note that the apodizer was omitted for these measurements, which is why the theoretical PIAA PSF is only at ~10^4 contrast).

The rows on Figure 8 correspond to an on-axis source and different off-axis positions (obtained by physically translating the fiber light). The left column on Figure 8 shows images with the PIAA lenses removed from our system (but

everything else the same), the middle column shows the images with the PIAA lenses in, and the rightmost column shows our models. Figure 9 shows horizontal slices of selected images. These comparisons demonstrate agreement between our models of an ideal system and measurements to better than ~10^{-3} contrast, below which we are starting to be affected by aberrations. However, clearly the main spot of the PSF is reasonably correct both for an on-axis as well as off-axis cases.

Our off-axis tests also serve as a calibration and validation of the angular scale on our images. Careful calibration of the angular scale (i.e. number of CCD pixels per λ/D on the sky), and in particular accurate measurements of the inner working angle of the system are very important because small gains in inner working angle lead to large gains in number of planets that can be found (the latter goes as the third power of the former). This scaling is trickier for PIAA than for many other coronagraphs because PIAA has an inherent magnification and distortion of off-axis sources. (The distortion is due to the fact that the PIAA lenses effectively distort the pupil plane and the magnification is due to the fact that the PIAA lenses compress the effective pupil plane size. Note that the distortion of the planetary PSFs appears more severe than it really is because of the logarithmic brightness stretch, and may actually be tolerable in a real system unless the planet is very far off-axis. Alternatively, this distortion can also be completely reversed after the star is blocked as in [3]). The magnification of our PIAA system is known through models (a factor of 2.272), but we also thought it prudent to measure the actual magnification and angular scale in our system to validate the models. We did this by first calibrating the amount of motion necessary to move our fiber light source by 1 λ/D with the PIAA system removed (which is trivial because the resulting Airy patterns are not distorted off-axis), and this effectively let us set the source position at known off-axis displacements in terms of λ/D. We then inserted the PIAA system and measured the displacements and profiles of the corresponding off-axis PSFs. As can be seen in the off-axis images and plots in Figures 8 and 9, the locations and distortions of the measured off-axis PSFs matched the models, validating that model-based calibration of the angular scale and inner working angle is correct. The "sky angular scale" thus obtained is used on most of the focal-plane images in this paper. (Note that this means that the images in the middle column of Figure 8 are actually 2.27 larger on the CCD than the left column.)

Another important calibration that needs to be performed is the photometry and location of the star, which is important both for contrast and inner working angle measurements, as well as for wavefront control. We do this regularly during wavefront control operations, using one of several of 3 methods, cross-referencing them from time to time. The first method is to put a sinusoidal ripple on the DM, and measure the locations and brightnesses of the corresponding diffraction orders appearing as speckles in the image. The second is to use already existing diffraction orders from the periodic print-through aberration on the DM (sometimes referred to as quilting). For our DM, the brightnesses of these "quilting diffraction orders" are known and don't vary appreciably with different patterns on the DM. For both of these methods, the location of the star is just the midpoint between two opposing diffraction orders. The third method is to use the star itself, which appears at 10^{-5} contrast after being attenuated by the focal plane occulter. All three of these methods have potential problems and sources of error, but when cross-referencing at least the second and third methods, they typically agree with each other to a few percent in contrast and 0.03 λ/D in location of the star, so that our contrast and inner working angle measurements are correct to 2 significant figures.

3.2 Wavefront control algorithms

We usually start a wavefront control run by applying a known voltage map to flatten the DM (obtained by Gavel et. al. at UCSC), or a DM map from a previous run, and then run one of two wavefront control algorithms: a variant of classical speckle nulling (SN, [15]), or the Electric Field Conjugation (EFC, [15]). SN is based on selecting a speckle in the dark zone, creating a sinusoidal ripple on the DM that would place a diffraction order on that speckle, and scanning the phase of that sinusoidal ripple until the diffraction order and speckle destructively interfere. This can be done with many speckles simultaneously per iteration (we typically use on the order of 50). Our variant of classical speckle nulling scans not only the phase, but also the amplitude of each ripple. In principle, the amplitude of each ripple necessary to maximally remove a particular speckle can be computed based on models, the contrast, and the location of that speckle. However, in practice we found that our models are sometimes inadequate given the presence of aberrations, and scanning the amplitude, although slower, can help. Speckle nulling is a very robust algorithm and has been used for the majority of our time spent on wavefront control. It also has the advantage that it does not require a model of the DM or the rest of the system to work, especially when scanning the amplitude of the DM ripples. All that is necessary is to calibrate the scale between the spatial frequency of the DM and the corresponding speckle location in the image plane. However, SN does have the drawback that it only creates spatial frequencies on the DM in the locations that correspond to the chosen dark zone. This tends to pile up light immediately outside the edge of the dark zone, which makes it

difficult to correct the edges. Sometimes the best way to correct the edges is to put spatial frequencies on the DM that fall outside the dark zone, and speckle nulling cannot do this directly (although it does happen as a side effect). This is where an algorithm such as EFC helps. EFC is based on measuring the phase and amplitude of speckles in the dark zone based on DM diversity, and then computing the DM pattern that will theoretically completely remove all light in the dark zone (or minimize the energy of the light if there are not enough degrees of freedom). This algorithm targets the entire dark zone in one shot and is thus much faster than speckle nulling (hours vs. minutes on our testbed). The pattern it puts on the DM is also the optimal one to correct everything in the dark zone, and usually does include putting spatial frequencies outside of the dark zone, helping with edge correction. In addition, EFC also produces an estimate of the "coherent" light in the image, i.e. that part of the light in the image that interferes with the central starlight in amplitude, as opposed to "incoherent" light, i.e. any part of the CCD image that appears to interfere in intensity (which can be an orthogonal polarization, or even a camera artifact, in addition to actual incoherent light). Determining what portions of the image correspond to coherent light and are thus correctable and what portions are incoherent is a very useful diagnostic tool. However, to work well, EFC requires good knowledge of the system model and in particular the model of the DM and the complex field in the plane of the DM. BMC DMs have been intensely studied at UCSC and can be modeled with reasonable accuracy, and the intensity of the DM field is relatively easy to measure (see Figure 7). The phase is not as simple, however. We measured it with a Gerchberg-Saxton type scheme based on CCD focus diversity, but the edges are a challenge to measure and seem a little too noisy at the moment. Presumably due to this effect, our EFC does not yet achieve as high of a contrast as speckle nulling does. So, our general approach so far has been to run the more robust speckle nulling, and then at appropriate times use EFC to target the edge of the dark zone as well as diagnose whether certain speckles are coherent (and thus correctable) or not.

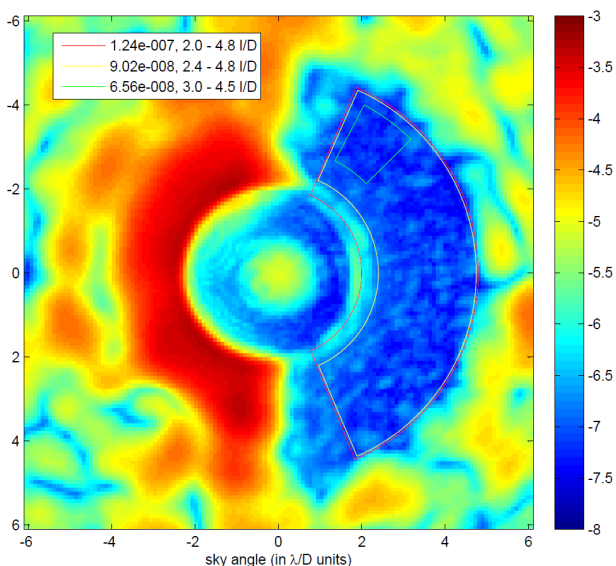### 3.3 High contrast results and analysis of limiting factors

Figure 10. CCD image showing 1.2 x 10^{-7} contrast between 2.0-4.8 λ/D.

Using the hardware and methods described above, we have demonstrated a contrast of 1.2×10^{-7} between 2.0 and 4.8 λ/D and 9.0×10^{-8} between 2.4 and 4.8 λ/D, both in almost a full half-plane. (Amplitude errors limit us from correcting the full plane, which requires 2 DMs.) Figure 10 shows the CCD image with these results. The contrast numbers here and elsewhere in our paper generally refer to the raw speckle contrast averaged across the dark zone in question. This corrected contrast represents a factor of about 5,000 improvement from the uncorrected contrast. Every decade of contrast improvement involved identification and elimination of several limiting factors. This process has proceeded at a steady pace and over the past half-year we have been improving contrast by about a factor of 2 every 6 weeks as we are eliminating each limiting factor.

As can be seen in Figure 10, the light around the edge of the focal plane occulter at 2 λ/D is relatively strong and is currently limiting our contrast at the inner working angle. This light is due to a combination of several effects that we have been investigating and improving over the past several months. Figure 11 demonstrates some of our investigations of limiting factors. The first (leftmost) plot shows one of our earlier SN runs where the light on the FPO edge is even stronger than in Figure 10. As explained in the previous section, we invoked EFC on the edge of the FPO to see if SN itself was the limit or something else. EFC indeed can dig deeper than SN around the edge of the FPO (see second image in Figure 11), but it too hit a limit, with the result that the rest of the light on the FPO edge is "incoherent", i.e. it seemed to modulate in intensity and not amplitude. As we investigated several potential sources of why this light is "incoherent", we found that to a large degree it is because it has a different polarization from the light that the DM creates there when it attempts to correct it. Introducing a polarizer before the CCD enables a better correction such as shown in the third figure. (Rotating the polarizer 90 degrees in this case while keeping the DM setting the same increases the light on the FPO edge by almost an order of magnitude to levels similar to the second image.) The exact source of this polarization effect is currently being investigated, but we do know that both the refractive PIAA system and the FPO have aberrations that are slightly polarization-dependent and are slightly birefringent. For the image in Figure 10, we had polarizers oriented parallel to each other immediately before the CCD and immediately upstream of the FPO. However, there is still light around the FPO edge in the third image of Figure 11 and according to EFC that light is again "incoherent". The limit we suspect here is the "Gibbs effect", or ringing of the light around the FPO on spatial scales smaller than a CCD pixel. Such ringing will be averaged in each pixel and appear as "incoherent" light to EFC. This high spatial frequency ringing can be low-pass filtered by an iris, or "lyot stop" between the FPO and the CCD. In the fourth image in Figure 11, a "lyot stop" is introduced in a plane conjugate to the DM between the FPO and the CCD, and EFC is run again. The effect is that the edge of the FPO is reduced by a factor of 2, suggesting that we are affected by the Gibbs' effect at some level. However, at time of this writing, we have not yet performed a similar test on our latest image (in Figure 10) with the "lyot stop", so it is not completely certain yet whether we are dominated by the Gibbs effect in FIgure 10, but probably all 3 of our latest limiting factors still play some role (the inefficiency of SN to correct the edge, imperfect control of polarization, Gibbs' effect). Another sequence of experiments similar to the one in Figure 11 will be necessary to determine this for sure and to reduce them further.
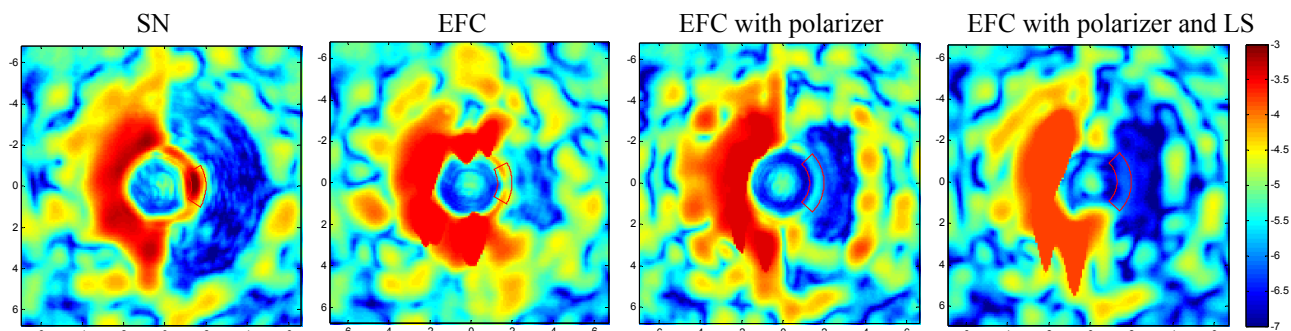

Figure 11. A sequence of tests designed to identify the source of the light around the edge of the focal plane stop and eliminate it

Another limiting factor that we are also starting to see is instability of the speckles. If all polarizers are removed, it turns out that the intensity of the speckles is quite stable (better than ~10^{-8} rms variations over 20 minutes) but with the polarizers in place, their intensity varies almost at the ~10^{-7} level. This has been recently traced to polarization instabilities at the fiber light source, which is due to random changes in the fiber outside our enclosure, where the environment is not especially stable. This can be mitigated by moving most of the fiber inside the enclosure and stabilizing better the part that is outside, and/or placing an additional polarizer in our layout.

4. CONCLUSIONS

The Phase-Induced Amplitude Apodization (PIAA) coronagraph is a high-performance coronagraph that can potentially enable the imaging of exo-Earths around nearby stars with a space telescope as small as 1.4m. It already has a successful track record of development and hardware demonstrations. A new laboratory at NASA Ames was established in 2008 for continued prototyping of the PIAA coronagraph and related technologies before eventual vacuum testing at JPL's High Contrast Imaging Testbed (HCIT). The testbed is being operated in a stabilized air environment, and is designed to

be flexible and cheap, with easy reconfiguration and quick turn-around of experiments. The initial goals pursued by the testbed are to demonstrate MEMS DM based wavefront control of the PIAA coronagraph, and to develop the environmental stability to be able to support very deep contrast levels. MEMS DMs' small size offers potentially critical advantages to space-based exoplanet missions which are usually size and mass constrained.

As of this writing, we have achieved 1.2e-7 contrast between 2.0 and 4.8 λ/D in monochromatic light. Contrast is improving at a steady rate as limiting factors are identified and eliminated. The main current limiting factors are believed to be a combination of polarization-dependent errors and polarization instabilities, and ringing on the occulter edge, both of which are starting to be controlled.

REFERENCES

1. Guyon O. "Phase-induced amplitude apodization of telescope pupils for extrasolar terrestrial planet imaging," A&A, 404, pp. 379-387 (2003).
2. Vanderbei R. J., Traub W. A., "Pupil Mapping in 2-D for High-Contrast Imaging," *Astrophysical Journal,* 665, pp794 – 798. (2005).
3. Pluzhnik E. A., Guyon O., Ridgway S. T., Martinache F., Woodruff R. A., Blain C., Galicher R., "Exoplanet Imaging with a Phase-Induced Amplitude Apodization Coronagraph III. Diffraction Effects and Coronagraph Design," *The Astrophysical Journal* 644, Issue 2, pp. 1246-1257. (2006).
4. Belikov R., Kasdin N.J., Vanderbei R.J., "Diffraction-based Sensitivity Analysis of Apodized Pupil-Mapping Systems," *ApJ* Vol 652, issue 1, pp. 833-844, 11/2006.
5. Vanderbei R., "Diffraction Analysis of 2-D Pupil Mapping for High-Contrast Imaging," *ApJ* Vol 636, p. 528, 2006.
6. Guyon O., Pluzhnik E. A, Kuchner M. J., Collins B., Ridgway S. T., "Theoretical Limits on Extrasolar Terrestrial Planet Detection with Coronagraphs," *Astrophysical Journal* 167, Issue 1, pp. 81-99 (2006).
7. Guyon O., Angel J.R.P., Belikov R., Egerman R., Gavel D., Give'on A., Greene T., Cahoy K., Kern B., Levine M., Ridgway S., Shaklan S., Tenerelli D., Vanderbei R., Woodruff R. A., "Detecting and Characterizing Exoplanets with a 1.4m space telescope: the Pupil mapping Exoplanet Coronagraphic Observer (PECO)," *Proc. of SPIE 7440* (2009).
8. Cahoy K., Guyon O., Schneider G., Marley M., Belikov R., Meyer M., Ridgway S., Traub W., Woolf N., "Science performance of the Pupil-mapping Exoplanet Coronagraphic Observer (PECO)," *Proc. of SPIE 7440* (2009).
9. Guyon O., Pluzhnik E., Martinache F., Totens J., Shinichiro T., Matsuo R., Blain C., Belikov R., "High Contrast Imaging and Wavefront Control with a PIAA Coronagraph: Laboratory System Validation," submitted to *PASP*, 2009.
10. Belikov R., et. al., "Overview of Technology Development for the Phase-Induced Amplitude Apodization (PIAA) Coronagraph," *Astro2010 decadal survey Technology Development White Paper, 2009.* (http://sites.nationalacademies.org/BPA/BPA_049522)
11. Guyon O., et. al., "Pupil mapping Exoplanet Coronagraphic Observer (PECO)," *Astro2010 Decadal Survey Notice of Interest, 2009.* (http://sites.nationalacademies.org/BPA/BPA_049519).
12. Kern B., Belikov R., Give'on A., Guyon O., Kuhnert A., Levine-West M. B., McMichael I. C., Mody D. C., Niessner A. F., Pueyo L., Shaklan S. B., Traub W. A., Trauger J. T., "Phase-Induced Amplitude Apodization (PIAA) coronagraph testing at the High Contrast Imaging Testbed," *Proc. of SPIE 7440* (2009).
13. Kasdin N. J., Vanderbei R. J., Littman M. G., Spergel D. N., "Optimal one-dimensional apodizations and shaped pupils for planet finding coronagraphy," *Applied Optics* 44(7), pp. 1117-1128 (2005).
14. Guyon O., Matsuo T., Angel R., "Coronagraphic Low-Order Wave-Front Sensor: Principle and Application to a Phase-Induced Amplitude Coronagraph," *ApJ,* Vol. 693, Issue 1, pp 75-84 (2009).
15. Trauger J. T., Gordon B. D., Kuhnert A. C., Moody D. C., Jr., Niessner A. F., Shi F., Wilson D. W., Burrows C. J., "Laboratory demonstration of high-contrast imaging technologies and algorithms for space coronagraphy," *Proc. of SPIE* 6693 (2007).
16. Give'on A., Belikov R., Shaklan S., and Kasdin J., "Closed loop, DM diversity-based, wavefront correction algorithm for high contrast imaging systems," Optics Express, Vol. 15, Iss. 19, pp. 12338-12343, 09/2007.